Title

Autotaxin through Lysophosphatidic Acid Stimulates Polarization, Motility, and Transendothelial Migration of Naive T Cells

Journal

The Journal of Immunology, 189(8)

ISSN

0022-1767

Authors

Zhang, Yafeng
Chen, Yi-Chun Maria
Krummel, Matthew F
et al.

Publication Date

2012-10-15

DOI

10.4049/jimmunol.1201604

Peer reviewed

Published in final edited form as:
J Immunol. 2012 October 15; 189(8): 3914–3924. doi:10.4049/jimmunol.1201604.

Autotaxin through lysophosphatidic acid stimulates polarization, motility, and transendothelial migration of naïve T cells

Yafeng Zhang[*], **Yi-Chun Maria Chen**[†], **Matthew F. Krummel**[†], and **Steven D. Rosen**[*]

[*]Department of Anatomy and Program in Immunology, University of California San Francisco, San Francisco, CA 94143

[†]Department of Pathology and Program in Immunology, University of California San Francisco, San Francisco, CA 94143

Abstract

Blood-borne lymphocytes home to lymph nodes by interacting with and crossing high endothelial venules (HEVs). The transendothelial migration (TEM) step is poorly understood. Autotaxin (ATX) is an ecto-enzyme that catalyzes the conversion of lysophosphatidylcholine (LPC) to lysophosphatidic acid (LPA), a bioactive lipid and a close relative of sphingosine-1-phosphate (S1P). HEVs produce and secrete ATX into the blood. A prior study has implicated ATX in the overall homing process but the step in which it functions and its mechanism of action have not been defined. Here, we show that HA130, an inhibitor of the enzymatic activity of ATX, slows T cell migration across lymph node HEVs *in vivo. Ex vivo*, ATX plus LPC or LPA itself induces the polarization of mouse naïve T cells and stimulates their motility on an ICAM-1 substratum. Under physiologic shear conditions in a flow chamber, LPA or ATX/LPC strongly enhances TEM of integrin-arrested T cells across an endothelial monolayer. HA130 blunts the TEM-promoting activity of ATX, paralleling its *in vivo* effects. T cells possess Mn^{+2}-activatable receptors for ATX, which are localized at the leading edge of polarized cells. ATX must bind to these receptors in order to elicit a maximal TEM response, providing a mechanism to focus the action of LPA onto arrested lymphocytes in flowing blood. Our results indicate that LPA produced via ATX facilitates T cell entry into lymph nodes by stimulating TEM, substantiating an additional step in the homing cascade. This entry role for LPA complements the efflux function of S1P.

INTRODUCTION

Lymphocyte migration (“homing”) from the blood into secondary lymphoid organs (SLO) is an essential step in lymphocyte recirculation, the process by which the repertoire of naïve lymphocytes rapidly cycles through SLOs, thereby enabling contact between sequestered antigens and rare cognate lymphocytes (1–3). For all SLOs except spleen, the portal of entry of blood-borne lymphocytes are high endothelial venules (HEVs) (1, 4, 5). These vessels are functionally specialized to capture lymphocytes from the flowing blood and to support their migration into SLOs. As is generally the case for leukocyte-endothelial cell (EC) interactions (6), naïve T cell recruitment across HEVs occur in several sequential steps: rolling of lymphocytes along the endothelium, arrest on the endothelium, intraluminal crawling, and finally trans-endothelial migration (TEM) into the SLO (4, 2, 5). In peripheral lymph node HEVs, the first step is mediated by transient interactions between L-selectin on lymphocytes and a complex of mucins on HEVs (7). The second step is due to “arrest” chemokines, such as CCL21, which are immobilized apically on HEVs (2, 5, 8). Signaling through CCR7, CCL21 activates αLβ2 on lymphocytes, which increases the integrin’s

Corresponding author: Steven Rosen, steven.rosen@ucsf.edu, phone: 415-476-1579; fax: 415-476-4845.

affinity for ICAM-1/ICAM-2 on HEVs, leading to the rapid arrest of the rolling cells (8, 9, 10). Some of the lymphocytes crawl intralumenally for several min before undergoing transendothelial migration (TEM), whereas the remainder undergo TEM without migration (11). TEM occurs within 2.5 min for T cells. (11). Shear stress provided by blood flow is required for both the integrin-mediated arrest and TEM steps (12, 13).

Previously, gene profiling of purified HEV-ECs unexpectedly revealed a very high expression of autotaxin (ATX) transcripts (14). ATX was initially discovered as a secreted protein from A2058 melanoma cells, which enhances their own motility (15). ATX is a ≈110 kDa protein with two amino-terminal somatomedin B-like domains, a phosphodiesterase domain, and a C-terminal nuclease-like domain (16, 17). ATX was later shown to be a lysophospholipase D, which catalyzes the conversion of lysophosphatidylcholine (LPC) to lysophosphatidic acid (LPA) (18). As an extracellular lysophospholipid, LPA engages 6 GPCRs (termed LPA1-6) and evokes diverse growth factor-like responses (motility, proliferation, survival, and differentiation) in multiple cell types (19, 20). LPA is now known to be responsible for the motility-promoting action of ATX on A2058 cells, as well as on other cancer and normal cells (21). ATX performs essential functions in vasculogenesis and neural tube formation during embryonic development (22, 23). In the adult, ATX is present in the blood and is responsible for the maintenance of LPA in plasma (22, 23). In mouse, the normal level of LPA is 200–400 nM (24) and in human 80–90 nM (25). Pathologic roles for ATX are indicated in cancer and cardiovascular disease (26, 27). In the context of immune function, ATX is over-expressed in synovial fibroblasts in rheumatoid arthritis and has been implicated in the pathogenic process (28). LPA acting through LPA2 inhibits dendritic cell activation and dampens allergic airway inflammation (29).

The discovery of abundant ATX transcripts in HEV-EC prompted two studies, which confirmed that ATX protein is expressed in HEVs of SLOs (30, 31). We further found that: 1) ATX is secreted apically by HEV-ECs; 2) ATX can bind to receptors on chemokine-activated T cells; 3) LPA is chemokinetic for T cells; and 4) injection of a catalytically inactive form of ATX (T210A) partially inhibits homing of T cells into SLOs (30). These findings led to a paracrine model of ATX function in homing (30) whereby ATX is secreted into the lumens of HEVs and binds to proximally-arrested T cells. The bound ATX uses the abundant LPC in the plasma (≈ 200 μM) to produce LPA, which promotes T cell entry into the lymphoid organ.

This speculative model has awaited further *in vivo* validation and a mechanistic understanding of how ATX and its enzymatic product LPA influence lymphocyte migration upon and across an endothelial substratum under physiologic shear stress conditions. The present study addresses these issues.

MATERIALS AND METHODS

Reagents

Mouse ICAM-1-Fc (796-IC-050), CCL21 (457-6C-025), and TNF-α (210-TA) were from R&D Systems, Minneapolis, MN. The antibodies used were: anti-CD44 (IM7; BD Biosciences, San Jose, CA), anti-CD3e (45-2C11; BD), anti-B220 (RA3-6B2; BD), anti-autotaxin AF5255; R&D), anti-CD49d (PS/2; Serotec, Raleigh, NC), anti-CD43 eBioR2/60; eBiosciences, San Diego, CA). Stock solutions of LPA were made in methanol (10 mM) and stored at −80°C. Dilutions into aqueous buffers were prepared just before use with methanol serving as the carrier control. We used 18:1 LPA for our studies, as it is naturally occurring in blood (24) and one of the enzymatic products of autotaxin (32). Fatty-acid free BSA (A8806), L-α-lysophosphatidylcholine (L4129), pertussis toxin, and Y-27632 were from

Sigma-Aldrich. BrP-LPA was from Echelon, Logan, UT. The biotinylation labeling Kit (704-0030) came from Novus, St. Charles, MO. Cy2-streptavidin (016-220-084) and Cy3–anti-rat IgG (712-166-150) were from Jackson ImmunoResearch, West Grove, PA.

Mice

All mouse protocols were approved by the UCSF Committee for Animal Research. For homing assays, C57BL/6 female mice (6–8 weeks, Charles River Labs, Wilmington, MA) were used. The following mice were from Jackson Laboratories: OTII, Ub-GFP, *Itgb2* null and *Itgb3* null. OTII-GFP mice were obtained by crossing OTII with Ub-GFP mice.

Cells

$CD3^+$ T cells were purified from mechanically-dispersed peripheral lymph nodes using the EasySep T cell Enrichment Kit (StemCell Tech, Vancouver, Canada). For motility assays, $CD4^+$ T cells were purified from PLNs of OTII Ub-GFP mice using EasySep Mouse $CD4^+$ T Cell Enrichment Kit (StemCell Tech). Purified cells were resuspended in RPMI plus 10% charcoal-dextran–treated FBS and incubated at 37°C ≈1 h before imaging. ≥90% of the $CD3^+$ cells and ≥95% of the $CD4^+$ T cells were naïve as defined by the criterion of $CD44^{lo}$. For most of the experiments, these populations are referred to as “naïve” T cells. TK1 cells were maintained in RPMI-1640 with 10% FBS, 100 units/ml penicillin, 100 μg/ml streptomycin, and 25 μM 2-mercaptoethanol.

T cell homing

Short-term homing of T cells was carried out as described (30). CFSE-labeled $CD3^+$ T cells (20×10^6 in 100 μl) without or with HA130 (2 nmoles per gram recipient mouse) in DMSO were injected intravenously into mice. HA130 or DMSO was reinjected at 7 and 12 min. At 15 min, SLOs were cryostat-processed for immunohistochemistry to highlight HEVs (MECA-79 staining for lymph nodes and CD31 staining for Peyer’s patches). The number of fluorescent lymphocytes “outside HEVs” (in the lymphoid organ parenchyma) and “within HEVs” (both in the lumens and walls) were counted. 2 mice were processed at a time (one HA130 and one control). 6 non-consecutive sections from 2 mesenteric lymph nodes (MLNs) and 3 peripheral lymph nodes (PLNs) of each mouse were evaluated. Ratios were determined for each section and a mean ratio was computed for each mouse. Means from 3 mice per group were combined to yield overall means ± SDs.

ATX/T210A preparation

The recombinant proteins were prepared as described previously (30).

Uropod assay

8-well chamber slides (154534; LabTek, Thermo, Rochester, NY) were coated with 3 μg/ml ICAM-1-Fc and CCL21 overnight. The slides were then blocked with 3% fatty acid-free BSA for 1h. TK1 lymphoma cells were cultured with 5% charcoal-dextran–treated FBS overnight. $CD3^+$ T cells were cultured with 10% charcoal-dextran–treated FBS for 2 h. Cells ($0.5 – 1 \times 10^6$) cells were added to the chamber (200 μl) containing HBSS buffer with 0.2% fatty acid-free BSA. LPA or ATX/LPC were added and cells were allowed to settle at 37°C. Attached cells were fixed with 4% formaldehyde in PBS. After washing and blocking with BSA, uropods were visualized by staining with (anti-CD44 or CD43) in combination with secondary antibodies. For Gαi or ROCK inhibition, cells were cultured for 2 h with PTX (200 ng/ml) or Y27632 (10 μM), respectively. For ATX inhibition experiments, cells were incubated with HA130 (0.3 μM) or BrP-LPA (10 μM) for 30 min prior to the addition of ATX.

Cell motility assays

Custom crawling chambers were assembled. Dividers for 6 chambers were made from Polydimethylsiloxane (Sylgard 184 Silicone Elastomer Kit, 10:1 mix, Midland, MI) formed in a printed mold. Each divider was then cut out by scalpel and placed on top of a glass slide (48311-703; VWR, Batavia, IL), and covered with a No.1 cover glass (48393-059; VWR) to create the chambers. For assays, the chambers were freshly coated with either 3 μg/ml ICAM-1/Fc with or without 400 ng/ml of CCL21 at 4°C overnight. The chambers were washed in PBS, blocked with PBS plus 0.5% fatty acid-free BSA, and kept in the blocking buffer until use. 5×10^4 OTII Ub-GFP $CD4^+$ T cells were resuspended in 100 μl block and seeded into the chamber. For LPA treatment, 1 μM LPA was added to the cells immediately before imaging. For the ATX/LPC treatment, cells were incubated with 1 μg/ml ATX for 5 min, followed by 10 μM LPC cells immediately before imaging. Imaging employed a Zeiss Axiovert 200M microscope with a plan-neofluor 20 x objective fitted with dual excitation and emission filter wheels and a Photometrics Coolsnap-HQ camera. Metamorph software (Universal Imaging, Molecular Devices, Sunnyvale, CA) was used for image acquisition and microscopic control. Images were collected in the GFP channel every 15 sec for 15 min. Image analysis and tracking employed Imaris software (Bitplane, South Windsor, CT).

ATX staining

To analyze ATX receptors, cells were incubated with a preformed complex of b-ATX (10 μg/ml) and PE-conjugated streptavidin (2 μg/ml) in HBSS buffer (with or without 0.5mM Mn^{+2}) at room temperature. T cells were gated by CD3 staining. PS/2 mAb (10 μg/ml) was used to block α4 integrin.

To analyze b-ATX distribution by immunofluorescence, TK1 cells on an ICAM-1 substratum were exposed to 0.1 μM LPA. Following fixation with 4% formaldehyde, washing and blocking, the cells were sequentially reacted with a complex of b-ATX/Cy2-streptavidin, and anti-CD44 with a Cy3-conjugated secondary antibody.

Transmigration under shear flow

BEnd.3 endothelial cells were grown to confluence in a 0.2% gelatin-coated BioFlux 48-well flow chamber plate (Fluxion Biosciences, S. San Francisco, CA). Monolayers were stimulated for 16 h with TNF-α (500 U/mL). CCL21 (1 μg/ml with 0.2% fatty acid-free BSA) was overlaid on the monolayer for 5 min followed by washing. T cells in HBSS with 0.2% fatty acid-free BSA were perfused for 2 min over the monolayer at 0.5 dyne/cm^2 and then flow was stopped for 5 min. The flow rate was then increased to 1 dyne/cm^2 for an additional 30 min. Images were recorded at 1 frame/10 sec by video recorder. The total number of arrested cells was determined after 10 min of flow. During the 30 min of flow, lymphocytes fell into 3 categories: 1) cells that moved less than 2 diameters (“static”); 2) cells that crawled ≥2 cell diameters without detaching/transmigrating (“crawling”); and 3) cells that became phase-contrast dark (“undergoing TEM”). In some experiments, HA130 (0.3 μM final) or BrP-LPA (10 μM final) was added. For competition with T210A, the chamber contained a 10-fold excess of T210A relative to the indicated amount of ATX.

Statistical analysis

The unpaired Student t-test was used to determine the statistical significance of pair-wise comparisons after satisfying t-test criteria (33) of equivalent variances and Gaussian distributions (approximately equal mean and median values). For comparisons of 3 or more groups, one-way ANOVA with the Tukey’s post-test was used.

RESULTS

HA130 inhibits homing of T cells

HA130 was recently identified as a potent small-molecule inhibitor of ATX (34). The inhibitor acts to reduce both the turnover number of ATX and its affinity for LPC. To accommodate the short half-life of HA130 in blood (≈ 3 min) (34), we employed a modified lymphocyte homing assay. We injected CFSE-labeled T cells together with HA130 intravenously into mice, and then re-injected the drug at 7 and 12 min. After 15 min, SLOs were sectioned and stained to reveal HEVs. $CFSE^+$ T cells were classified as either "outside HEVs" (in the lymphoid organ parenchyma) or "within HEVs" (luminal or in HEV walls). The ratio of "outside HEVs" to "inside HEVs" was used as index of T cell migration across HEVs. In Peyer's patches, very few cells migrated into the parenchyma in 15 min, so the action of HA130 could not be evaluated. However, for peripheral lymph nodes (PLNs) and mesenteric lymph nodes (MLNs), many cells had migrated into the parenchyma (Fig. 1A). HA130 decreased the "outside HEVs/inside HEVs" ratio by 3–4-fold, compared to vehicle-treated animals vehicle (Fig. 1B, $p < 0.01$ for both PLNs and MLNs). This result is consistent with HA130 retarding the migration of T cells across LN HEVs.

LPA and ATX/LPC polarize naïve T cells

LPA induces chemokinesis of T cells in transwell assays (30). We sought to investigate the cellular mechanisms by which LPA was exerting these effects. Stam et al. (35) previously reported that LPA induced the formation of pseudopods in a lymphoma cell line. To extend these findings, we examined the effects of LPA, as well as ATX, on T cells. Whereas T cells in the blood are round, T-cells that have entered a tissue exhibit an amoeboid "hand-mirror" morphology, which is characterized by a broad leading edge, a cell body with the nucleus, and a uropod at the tail (9, 36, 37). We first asked whether LPA at concentrations previously shown to be active in transwell assays (30) could induce the polarization of TK1 cells, a mouse $CD8^+$ T cell line (38). We quantified this response by monitoring the accumulation of CD44 in uropods (37). TK1 cells were mixed with LPA at varying concentrations and allowed to settle on an ICAM-1 substratum. With no added LPA, 10% of the cells were polarized by 7 min (Figs. 2A, B). At 0.1 μM, the polarization was 48% and reached 78% at 10 μM. LPA at 1 μM induced maximal polarization within 5 min with no detectable fall-off after 30 min, indicating the absence of desensitization over this period (Fig. 2C).

We next investigated primary $CD3^+$ T cells, which were isolated by negative selection from LNs. At least 90% of these cells were naïve defined by the criterion of $CD44^{lo}$ (not shown), and we refer to this population as naïve. LPA also induced polarization of these cells (Fig. 2D) with uropods identified by CD43 staining (37). LPA at 10 μM induced polarization to a maximum of 32%. Alon and coworkers (39) have reported that immobilized CCL21 causes rapid polarization and motility of T cells on an adhesive substratum. We therefore asked what effect LPA would have on T cells that were simultaneously exposed to CCL21, which was co-immobilized with ICAM-1. CCL21 alone (200 ng/ml) induced polarization of naïve T cells to 21% (Fig. 2D). Adding LPA increased the level of polarization to a level of 58% at 10 μM LPA. A 2-fold higher level of CCL21 did not produce further augmentation (not shown). Thus, soluble LPA and immobilized CCL21 act additively to promote uropod formation in naïve T cells.

As ATX catalyzes the production of LPA, we wanted to determine if ATX could also induce the polarization of T cells. When we added ATX (5 μg/ml) to TK1 cells on an ICAM-1 substratum, we observed uropod formation in the presence of LPC but not in its absence (Fig. 3A). LPC at 10 μM was more effective than 1 μM. The IC_{50} for ATX in this assay was ≈ 0.2 μg/ml. Notably, the response to ATX/LPC was very rapid. After 30 sec of exposure to

1 μg/ml of ATX, the polarization of TK1 cells doubled to 34% relative to the baseline level (Fig. 3B). By 10 min, the level of polarization reached ≈75%, which was largely sustained for another 20 min.

To verify the importance of the enzymatic activity of ATX, we tested an enzymatically inactive form (T210A). There was no uropod inducing activity by T210A at 5 μg/ml in the presence of LPC (1 μM) (Fig. 3A). We also tested two small-molecule inhibitors of ATX: HA130 (see above) and BrP-LPA (40). The latter compound is a bromophosphonate analogue of LPA, which is a low micromolar inhibitor (IC50 = ≈ 0.1 μM) of ATX and antagonizes several of the LPARs (40). HA130 at 0.3 μM and BrP-LPA at 10 μM completely ablated the activity of ATX on TK1 uropod formation (Fig. 3C). However, neither had any effect on LPA-induced uropods. Thus, we conclude that BrP-LPA was able to block ATX-induced uropods by inhibiting ATX rather than LPA antagonism, which is consistent with the fact that BrP-LPA does not block all LPA receptors (40). Pretreatment of TK1 cells with 200 ng/ml pertussis toxin (PTX) did not diminish ATX-induced polarization, indicating that the Gαi subfamily of G-proteins was not involved in this response (Fig. 3D). Y27632 is a pharmacologic inhibitor of ROCK, a kinase which regulates myosin contractility (11). ROCK is an effector of RhoA, which is downstream of Gα12/13 G-proteins (41). Incubation of TK1 cells with Y27632 (10 μM) completely blocked the induction of uropods by ATX (Fig. 3D).

We next examined primary naïve $CD3^+$ T cells and found that ATX in combination with LPC also induced their polarization (Fig. 3E). As with LPA, the action of ATX on uropod formation was additive with that of immobilized CCL21. Without LPC, ATX did not augment polarization. ATX, as well as LPA, also induced the polarization of primary human T cells and neutrophils from peripheral blood (Fig. 3F). Neutrophil polarization by LPA has been previously reported (42).

ATX Receptors on T cells

Our previous work showed that human T cells can bind to plastic-immobilized ATX in an α4β1-dependent manner (30). We found that CCL21 stimulation of T cells or the addition of Mn^{+2} (which globally activate integrins) greatly augmentsα4β1-dependent binding, suggesting that ATX binding requires the active conformation of α4β1 (30). Similarly, activated β1 and β3 integrins on platelets are required to bind ATX (43). Although Mn^{+2} increases the binding of mouse T cells to immobilized ATX, we were unable to implicate the involvement of any particular integrin (30) To further study ATX receptors on lymphocytes, we linked biotin to ATX (b-ATX) to generate a soluble probe. Consistent with previous observations (30), naïve $CD3^+$ T cells showed increased b-ATX staining in the presence of Mn^{+2} (Fig. 4A), as did $CD4^+$ and $CD8^+$ subsets of T cells as well as B cells (Supplementary Fig. 1). A neutralizing antibody to α4β1 (PS/2) did not diminish staining of T cells (Fig. 4B), and T cells from β2 and β3 null mice did not show reduced staining as compared to wild type T cells (Fig. 4C). b-ATX staining of T cells was >90% inhibited by the addition of a 10-fold excess of T210A, verifying that the receptors were saturable (Fig. 4D). Staining of rounded TK1 cells with b-ATX revealed a patchy distribution around the cells. Upon LPA-induced polarization of TK1 cells, b-ATX staining was greatly enriched at the leading edge of cells opposite from the CD44-stained uropod (Fig. 4E).

LPA and ATX/LPC induce motility of naïve T cells

As a polarized morphology is a requirement for active leukocyte migration (36, 9, 37), we performed motility assays. Here, we used CD4+ T cells of which ≥95% were naïve. Using a custom chamber for visualizing 2-D cell behavior, we found that 1 μM LPA augmented $CD4^+$ T cell migration on a substratum of co-immobilized ICAM-1 and CCL21 (Fig. 5).

LPA induced a 26% fold increase in median velocity from 4.72 um/min to 5.96 μm/min ($p < 0.0001$, Fig. 5A). Furthermore, the LPA-treated cells exhibited a marked shift to lower median turning angles (81.3° vs. 51.1°, $p<0.0001$) (Fig. 5B), indicating a greater tendency to move in a straight line. These effects persisted for at least 60 min following exposure to LPA (not shown).

We next investigated ATX in the migration chamber (Fig. 6). Consistent with the previous report (39), immobilized CCL21 promoted naïve T cell migration on ICAM-1, as measured by increased velocity (2.43 μm/min vs. 5.49 μm/min, $p <0.001$) (Fig. 6E), decreased turning angles (90.2° vs. 76.8°, $p <0.001$) (Fig. 6F), and increased net displacement (2.73 μm/10 min vs. 13.9 μm/10 min, $p <0.001$) (Fig. 6G). Similarly, ATX/LPC produced comparable effects on velocity (2.43 μm/min vs. 4.59 μm/min, $p <0.001$) (Fig. 6E), turning angle (90.2° vs. 68.5°, $p <0.001$) (Fig. 6F), and net displacement (2.73 μm/10 min vs. 15.2 μm/10 min, $p <0.001$) (Fig. 6G) of T cells, as compared to the no-stimulant condition. Finally, the effects of both treatments together on migration were additive. The median velocity of 8.05 μm/min (with 25% above 11.05 μm/min) in the presence of both stimulants (Fig. 6E) compares to median velocities of 5.7–15.1 μm/min observed for interstitial T cell migration within lymph nodes (44–46). Our findings establish that naïve T cell polarization induced by LPA or ATX/LPC is indeed translated into motility.

LPA and ATX/LPC promote TEM of T cells under shear stress

Arrested lymphocytes on HEVs experience the shear-stress of blood flow as they crawl on the luminal aspects of the endothelium prior to TEM. We turned to a previously described *ex vivo* system to investigate lymphocyte migration on an EC monolayer and TEM under physiologic shear flow (13, 47). In this design, bEnd.3 endothelial cells are cultured on the bottom of a flow chamber and treated with TNF-α to induce expression of integrin counter-receptors. The EC monolayer is apically exposed to an “arrest” chemokine, such as CCL21 or CXCL12, and lymphocytes are allowed to interact with the monolayer at low shear stress. This step circumvents the physiologic rolling step in which slowly moving lymphocytes encounter arrest chemokines. Upon application of shear stress to the system, the lymphocytes stick via activated integrins (13). They then undergo TEM with the vast majority of the cells crossing the endothelial barrier by the paracellular route (47). We allowed $CD3^+$ T cells to settle on TNF-α activated and CCL21-coated bEnd.3 ECs and then applied shear (1 dyne/cm^2). After 10 min, we observed robust shear-resistant adhesion of T cells (Fig. 7A). Without CCL21 treatment, five-fold fewer T cells bound to the monolayer. Consistent with previous findings (13), inclusion of an anti-β2 mAb reduced the number of adherent cells (shear-resistant) by ≈75%, and the further addition of anti-MAdCAM-1 mAb reduced adhesion by 95%. After an additional 20 min of flow, ≈5% of the adherent T cells had completed TEM, as judged by the appearance of phase-dark cells under the monolayer. When we added LPA to the chamber, there was a dose-dependent increase in the number of transmigrated cells from 5% with no added LPA to 20% with 10 μM LPA (Fig. 7B). With ATX added instead of LPA, there was a dose-dependent increase in TEM in the presence of LPC. 1 μg/ml ATX with 1 μM LPC produced a 6-fold increase to 30% (Fig. 7C). Without LPC, ATX did not change the level of TEM from the baseline, and conversely LPC without ATX also had no effect. Categorizing the behavior of cells, we found that 1 μg/ml ATX (1 μM LPC) reduced the % of static T cells by more than 50% and increased the % of cells undergoing TEM by 6-fold without altering the % of cells that crawled intraluminally (Fig. 7D). To substantiate that ATX enzymatic activity was essential, we tested the T210A mutant and found that it was inactive at 5 μg/ml (Fig. 7E). Furthermore, both HA130 and BrP-LPA abolished the enhancing effect of ATX on TEM (Fig. 7E). However, BrP-LPA had no effect on LPA-induced TEM (data not shown). To confirm that naïve cells within the $CD3^+$ T cell population were responding in this assay, we further purified the cells by negative selection

for CD44. ATX/LPC induced the same extent of TEM by this enriched population (≥ 99% naïve), as observed for parental cells (90% naïve). (Supplementary Fig. 2)

The bEnd.3 system provided the opportunity to model the previous *in vivo* observation that intravenous injection of T210A markedly reduced T cell homing (30). Our interpretation was that the inactive ATX displaced endogenous ATX from T cells and prevented the local production of motility-enhancing LPA in the vicinity of the cells. Since T210A competes the binding of ATX to T cells (Fig. 4D), inclusion of an excess of T210A relative to ATX in the flow chamber allowed us to determine whether the active enzyme had to bind to T cells in order to stimulate TEM. We tested two concentration of ATX with or without a 10-fold excess of T210A (Fig. 7F). At 5 μg/ml of ATX, 28% of the arrested T cells completed TEM during the 30 min period of flow. The inclusion of 50 μg/ml of T210A reduced TEM to 16%. ATX at 0.5 μg/ml stimulated 12% TEM. Inclusion of 5 μg/ml of T210A reduced TEM to the background level. These results indicate that binding of ATX to T cells is required for optimal TEM-promoting activity.

DISCUSSION

Our previous study demonstrated the activity of LPA on primary mouse and human T cells in a transwell assay (30). As lymphocytes normally migrate in contact with other cells (e.g., endothelium) or extracellular matrix, the transwell assay was not informative as to whether LPA could induce motility responses in T cells on a biologically relevant substratum. In the present investigation, we found that LPA promoted the transformation of T cells on an ICAM-1 substratum from a rounded shape to a polarized morphology with a well-defined leading edge and uropod (Fig. 2). The distinctive hand-mirror morphology is a prerequisite for active cell migration of leukocytes (36, 37). Consistent with this, we verified that LPA induced motility of naïve T cells on an ICAM-1 substratum (Fig. 5). Surface-bound CCL21 also promoted motility of these cells, as previously reported (39), and soluble LPA and immobilized CCL21 functioned additively.

It was critical to determine whether ATX could serve as a source of LPA in these assays. Indeed, ATX/LPC added to TK1 cells efficiently induced their polarization (Fig. 3). PTX treatment had no effect on this response, in contrast to its abrogation of CCL21-induced polarization and motility of lymphocytes (39). ATX/LPC was also active on naïve T cells, inducing both their polarization and motility, and these cells also responded additively to CCL21 and ATX/LPC (Figs. 3, 6). Several studies have reported that the random migration of T cells within lymph nodes strongly depends on Gαi signaling (44, 45). Contributing to this motility are CCR7 and its ligands (CCL21 and CCL19) (44–46). Interestingly, a component of T cell motility remains after complete PTX inhibition of Gαi signaling, implicating a chemokine-independent mechanism (44, 45). Notably, ATX transcripts and protein are detected within the parenchyma of LNs apart from their very high expression in HEVs (30). A question for further work is whether LPA produced by extravascular ATX influences the migration and positioning of lymphocytes within lymphoid organs.

While the above findings have implications for extravascular migration of lymphocytes under no-shear conditions, our primary interest was the contribution of ATX/LPA to T cell interactions with HEVs under blood flow conditions. To model these events, we employed cytokine-activated bEnd.3 ECs in a flow chamber with apically-displayed CCL21 (Fig. 7). Previous work with this model has documented integrin-dependent sticking of lymphocytes, followed by a migratory phase in the which lymphocytes polarize, migrate on the EC surface, and finally undergo TEM (13, 47). The timing and molecular requirements for these steps in this *ex vivo* system closely parallel those established for T cell homing across HEVs *in vivo* (11, 48, 49).

Employing this system, we found that LPA or ATX/LPC induced a 4–6 fold increase in naïve T cells that underwent TEM. Interestingly, the number of crawling cells was not increased by exposure to ATX/LPC. Thus under flow ATX does not appear to affect the conversion of arrested cells to migrating cells but rather increases the efficiency of TEM. Of note, Park et al. (49) found that mutant T cells which are unable to down-regulate LFA-1 affinity exhibit reduced diapedesis across HEVs. Furthermore, pharmacologic impairment of uropod contractility slows TEM of T cells across both HEVs *in vivo* and cultured endothelium, probably because release of the adherent uropod is impaired (11, 50). These studies highlight the importance of integrin de-adhesion during lymphocyte TEM and raise the possibility that LPA signaling may be involved in down-regulation of LFA-1 affinity.

ATX is a large multidomain protein, and it is conceivable that it could modulate T cell migration through a non-enzymatic mechanism. In fact, Zhao et al. (51) found that T210A could stimulate the motility of airway epithelial cells. We established that ATX was exerting its effects on T cell TEM via its enzymatic activity by showing that there was no TEM promoting activity by: LPC alone, ATX in the absence of LPC, or T210A. Furthermore, both HA130 and BrP-LPA completely blocked the ability of ATX to promote TEM. This *ex vivo* finding with HA130 complements the observation that this ATX antagonist also impeded the migration of T cells of lymphocytes across HEVs *in vivo*.

ATX was originally thought to be a type II transmembrane protein and was proposed to be released from the cell surface by shedding (16). Subsequently, ATX was shown to be a true secretory protein, which is processed at its amino terminus by the removal of a signal sequence and furin-mediated cleavage (17). We employed b-ATX to verify the presence of ATX receptors on mouse T cells (Fig. 4). Though ATX binding was enhanced by Mn^{+2}, we could not directly implicate the involvement of particular integrins, as has been done for human T cells ($\alpha 4\beta 1$) (30) and platelets ($\beta 1$ and $\beta 3$) (43).

Nonetheless, we were still able to support the functional relevance of ATX binding to T cells in the bEnd.3 system. Thus, we found that ATX-stimulated TEM was markedly reduced when the ATX was added in the presence of a 10-fold excess of T210A, a condition which reduced the level of ATX associated with the surface of T cells but did not change the amount of active enzyme in the flow chamber (Fig. 7). This *ex vivo* result rationalizes and complements the previous *in vivo* demonstration that intravenous administration of T210A inhibits lymphocyte homing (30).

Two mutually non-exclusive mechanisms can be envisioned for how ATX binding to T cells potentiates its TEM-promoting activity. Firstly, the crystal structure of ATX reveals a hydrophobic channel, which is thought to serve as conduit for the passage of LPA from the active site of the enzyme to an exit site on the surface of the enzyme (52, 53). As the exit site is predicted to be at the interface of ATX with its cellular binding partner, the hydrophobic channel could be the basis for a shuttling mechanism to transfer LPA close to its signal transduction receptors on the partner cell (52, 53). Notably, we detected ATX binding at the leading edge of lymphocytes where many chemo-receptors are localized (37). An additional refinement to enhance signaling would be an actual physical association between ATX and the LPAR. In fact, lung epithelial cells, which migrate in response to ATX, exhibit a cell surface complex of ATX with LPA1 and $\beta 4$ integrin (51). The existence of an analogous complex on lymphocytes would be predicted to facilitate shuttling of LPA to its LPARs so as to counteract the dissipative action of blood flow on focally generated LPA and to sequester LPA from the action of lipid phosphate phosphatases in the blood. A second possible mechanism for potentiation is that the interaction of ATX with its receptors on T cells activates the enzyme, as appears to occur when ATX binds to activated platelets (43).

Although the present study establishes an important role for the ATX-LPA signaling axis in T cell migration, the relevant LPARs remain to be identified. Of the 6 LPARs, 4 (LPA2, LPA4, LPA5, and LPA6) are expressed at the transcript level in populations of mouse T cells as determined by mining of the Immunological Genome Project database (www.immgen.org). Functions other than cell migration are served by lymphocyte LPARs, for example in cytokine secretion, cell proliferation, and cell survival (54). TK1 cells express transcripts for LPA2, LPA5, and LPA6 (data not shown). As Y27632 prevented the polarization response of this cell type to ATX/LPC (Fig. 3D), the Gα12/13–Rho axis is implicated in the signaling pathway (41). All three of the LPARs present in TK1 cells can couple to this class of G-proteins (19, 55). Importantly, our findings that 10 μM BrP-LPA did not inhibit either LPA-induced polarization or LPA-induced TEM argues against the involvement of LPA1-4 in these responses, since BrP-LPA antagonizes these receptors with submicromolar Ki's (56). Interestingly, BrP-LPA is a weak agonist of LPA5 (40). Thus, LPA5 and LPA6 (not yet investigated with BrP-LPA) are of particular interest with respect to their potential roles in the polarization and TEM of T cells. Clearly, the endothelium is not a passive partner during TEM, and locally produced LPA may also signal through LPARs on endothelial cells during the process (31).

Sphingosine-1-phosphate (S1P) and LPA are closely related lysophospholipids, both having a 3 carbon scaffold, a phosphate head group, and a single fatty acid chain (20). Like LPA, S1P signals through multiple GPCRs (20). Notably, S1P regulates the efflux of lymphocytes from lymph nodes into lymph (57, 58). The present study substantiates a role for LPA in the entry of blood-borne lymphocytes into lymph nodes and thus expands the functions of extracellular lysophospholipids in leukocyte trafficking.

Supplementary Material

Refer to Web version on PubMed Central for supplementary material.

Acknowledgments

This work was supported by grants from the NIH to SDR (RO1-GM57411 and RO1-GM23547) and to MK (AI52116). Y Z. was supported by a postdoctoral fellowship from the American Heart Association (A115033).

We are grateful to Drs. Harald Albers, Huib Ovaa, and Wouter Moolenaar of the Netherlands Cancer Institute for generously providing HA130 prior to its commercial availability. Preliminary experiments on LPA-induced polarization of lymphocytes were conducted by Hidenobu Kanda and Yuka Morita.

Abbreviations used

ATX	autotaxin
EC	endothelial cell
HEV	high endothelial venule
LPC	lysophosphatidylcholine
LPA	lysophosphatidic acid
LPAR	LPA receptor
MLN	mesenteric lymph node
PLN	peripheral lymph node
PTX	pertussis toxin
S1P	sphingosine 1 phosphate

SLO	secondary lymphoid organ
TEM	transendothelial migration

References

1. Gowans JL, Knight EJ. The route of recirculation of lymphocytes in the rat. Proc R Soc Lond Ser B. 1964; 159:257–282. [PubMed: 14114163]
2. Butcher EC, Picker LJ. Lymphocyte homing and homeostasis. Science. 1996; 272:60–66. [PubMed: 8600538]
3. Ruddle NH, Akirav EM. Secondary lymphoid organs: responding to genetic and environmental cues in ontogeny and the immune response. J Immunol. 2009; 183:2205–2212. [PubMed: 19661265]
4. Girard JP, Springer TA. High endothelial venules: specialized endothelium for lymphocyte migration. Immunol Today. 1995; 16:449–457. [PubMed: 7546210]
5. von Andrian UH, Mempel TR. Homing and cellular traffic in lymph nodes. Nat Rev Immunol. 2003; 3:867–878. [PubMed: 14668803]
6. Ley K, Laudanna C, Cybulsky MI, Nourshargh S. Getting to the site of inflammation: the leukocyte adhesion cascade updated. Nat Rev Immunol. 2007; 7:678–689. [PubMed: 17717539]
7. Rosen SD. Ligands for L-selectin: homing, inflammation, and beyond. Ann Rev Immunol. 2004; 22:129–156. [PubMed: 15032576]
8. Alon R, Shulman Z. Chemokine triggered integrin activation and actin remodeling events guiding lymphocyte migration across vascular barriers. Exp Cell Res. 2011; 317:632–641. [PubMed: 21376176]
9. Thelen M, Stein JV. How chemokines invite leukocytes to dance. Nat Immunol. 2008; 9:953–959. [PubMed: 18711432]
10. Hogg N, Patzak I, Willenbrock F. The insider's guide to leukocyte integrin signalling and function. Nat Rev Immunol. 2011; 11:416–426. [PubMed: 21597477]
11. Soriano SF, Hons M, Schumann K, Kumar V, Dennier TJ, Lyck R, Sixt M, Stein JV. In vivo analysis of uropod function during physiological T cell trafficking. J Immunol. 2011; 187:2356–2364. [PubMed: 21795598]
12. Cinamon G, Shinder V, Alon R. Shear forces promote lymphocyte migration across vascular endothelium bearing apical chemokines. Nat Immunol. 2001; 2:515–522. [PubMed: 11376338]
13. Shulman Z, Pasvolsky R, Woolf E, Grabovsky V, Feigelson SW, Erez N, Fukui Y, Alon R. DOCK2 regulates chemokine-triggered lateral lymphocyte motility but not transendothelial migration. Blood. 2006; 108:2150–2158. [PubMed: 16772603]
14. Palmeri D, Zuo FR, Rosen SD, Hemmerich S. Differential gene expression profile of human tonsil high endothelial cells: implications for lymphocyte trafficking. J Leuk Biol. 2004; 75:910–927.
15. Stracke ML, Krutzsch HC, Unsworth EJ, Arestad A, Cioce V, Schiffmann E, Liotta LA. Identification, purification, and partial sequence analysis of autotaxin, a novel motility-stimulating protein. J Biol Chem. 1992; 267:2524–2529. [PubMed: 1733949]
16. Murata J, Lee HY, Clair T, Krutzsch HC, Arestad AA, Sobel ME, Liotta LA, Stracke ML. cDNA cloning of the human tumor motility-stimulating protein, autotaxin, reveals a homology with phosphodiesterases. J Biol Chem. 1994; 269:30479–30484. [PubMed: 7982964]
17. Jansen S, Stefan C, Creemers JWM, Waelkens E, van Eynde A, Stalmans W, Bollen M. Proteolytic maturation and activation of autotaxin (NPP2), a secreted metastasis-enhancing lysophospholipase D. J Cell Sci. 2005; 118:3081–3089. [PubMed: 15985467]
18. Umezu-Goto M, Kishi Y, Taira A, Hama K, Dohmae N, Takio K, Yamori T, Mills GB, Inoue K, Aoki J, Arai H. Autotaxin has lysophospholipase D activity leading to tumor cell growth and motility by lysophosphatidic acid production. J Cell Biol. 2002; 158:227–233. [PubMed: 12119361]
19. Choi JW, Herr DR, Noguchi K, Yung YC, Lee CW, Mutoh T, Lin ME, Teo ST, Park KE, Mosley AN, Chun J. LPA receptors: subtypes and biological actions. Ann Rev Pharm Tox. 2010; 50:157–186.

20. Blaho VA, Hla T. Regulation of mammalian physiology, development, and disease by the sphingosine 1-phosphate and lysophosphatidic acid receptors. Chem Rev. 2011; 111:6299–6320. [PubMed: 21939239]
21. Okudaira S, Yukiura H, Aoki J. Biological roles of lysophosphatidic acid signaling through its production by autotaxin. Biochimie. 2010; 92:698–706. [PubMed: 20417246]
22. Tanaka M, Okudaira S, Kishi Y, Ohkawa R, Iseki S, Ota M, Noji S, Yatomi Y, Aoki J, Arai H. Autotaxin stabilizes blood vessels and is required for embryonic vasculature by producing lysophosphatidic acid. J Biol Chem. 2006; 281:25822–25830. [PubMed: 16829511]
23. van Meeteren LA, Ruurs P, Stortelers C, Bouwman P, van Rooijen MA, Pradere JP, Pettit TR, Wakelam MJ, Saulnier-Blache JS, Mummery CL, Moolenaar WH, Jonkers J. Autotaxin, a secreted lysophospholipase D, is essential for blood vessel formation during development. Mol Cell Biol. 2006; 26:5015–5022. [PubMed: 16782887]
24. Tomsig JL, Snyder AH, Berdyshev EV, Skobeleva A, Mataya C, Natarajan V, Brindley DN, Lynch KR. Lipid phosphate phosphohydrolase type 1 (LPP1) degrades extracellular lysophosphatidic acid in vivo. Biochem J. 2009; 419:611–618. [PubMed: 19215222]
25. Kishimoto T, Matsuoka T, Imamura S, Mizuno K. A novel colorimetric assay for the determination of lysophosphatidic acid in plasma using an enzymatic cycling method. Clin Chim Acta. 2003; 333:59–67. [PubMed: 12809736]
26. Smyth SS, Cheng HY, Miriyala S, Panchatcharam M, Morris AJ. Roles of lysophosphatidic acid in cardiovascular physiology and disease. Biochim Biophys Acta. 2008; 1781:563–570. [PubMed: 18586114]
27. Houben AJ, Moolenaar WH. Autotaxin and LPA receptor signaling in cancer. Can Metas Rev. 2011; 30:557–565.
28. Nikitopoulou I, Oikonomou N, Karouzakis E, Sevastou I, Nikolaidou-Katsaridou N, Zhao Z, Mersinias V, Armaka M, Xu Y, Masu M, Mills GB, Gay S, Kollias G, Aidinis V. Autotaxin expression from synovial fibroblasts is essential for the pathogenesis of modeled arthritis. J Exp Med. 2012; 209:925–933. [PubMed: 22493518]
29. Emo J, Meednu N, Chapman TJ, Rezaee F, Balys M, Randall T, Rangasamy T, Georas SN. Lpa2 Is a negative regulator of both dendritic cell activation and murine models of allergic lung inflammation. J Immunol. 2012; 188:3784–3790. [PubMed: 22427635]
30. Kanda H, Newton R, Klein R, Morita Y, Gunn MD, Rosen SD. Autotaxin, an ectoenzyme that produces lysophosphatidic acid, promotes the entry of lymphocytes into secondary lymphoid organs. Nat Immunol. 2008; 9:415–423. [PubMed: 18327261]
31. Nakasaki T, Tanaka T, Okudaira S, Hirosawa M, Umemoto E, Otani K, Jin S, Bai Z, Hayasaka H, Fukui Y, Aozasa K, Fujita N, Tsuruo T, Ozono K, Aoki J, Miyasaka M. Involvement of the lysophosphatidic acid-generating enzyme autotaxin in lymphocyte-endothelial cell interactions. Am J Pathol. 2008; 173:1566–1576. [PubMed: 18818380]
32. Wijesinghe DS, Mayton EK, Mietla JA, Mukherjee A, Wu J, Fang X, Chalfant CE. Characterization of lysophosphatidic acid subspecies produced by autotaxin using a modified HPLC ESI-MS/MS method. Anal Meth. 2011; 3:2822–2828.
33. Lamb TJ, Graham AL, Petrie A. T testing the immune system. Immunity. 2008; 28:288–292. [PubMed: 18341999]
34. Albers HM, Dong A, van Meeteren LA, Egan DA, Sunkara M, van Tilburg EW, Schuurman K, van Tellingen O, Morris AJ, Smyth SS, Moolenaar WH, Ovaa H. Boronic acid-based inhibitor of autotaxin reveals rapid turnover of LPA in the circulation. Proc Natl Acad Sci U S A. 2010; 107:7257–7262. [PubMed: 20360563]
35. Stam JC, Michiels F, van der Kammen RA, Moolenaar WH, Collard JG. Invasion of T-lymphoma cells: cooperation between Rho family GTPases and lysophospholipid receptor signaling. EMBO J. 1998; 17:4066–4074. [PubMed: 9670021]
36. Krummel MF, Macara I. Maintenance and modulation of T cell polarity. Nat Immunol. 2006; 7:1143–1149. [PubMed: 17053799]
37. Sanchez-Madrid F, Serrador JM. Bringing up the rear: defining the roles of the uropod. Nat Rev Mol Cell Biol. 2009; 10:353–359. [PubMed: 19373240]

38. Evans SS, Wang WC, Bain MD, Burd R, Ostberg JR, Repasky EA. Fever-range hyperthermia dynamically regulates lymphocyte delivery to high endothelial venules. Blood. 2001; 97:2727–2733. [PubMed: 11313264]
39. Woolf E, Grigorova I, Sagiv A, Grabovsky V, Feigelson SW, Shulman Z, Hartmann T, Sixt M, Cyster JG, Alon R. Lymph node chemokines promote sustained T lymphocyte motility without triggering stable integrin adhesiveness in the absence of shear forces. Nat Immunol. 2007; 8:1076–1085. [PubMed: 17721537]
40. Zhang H, Xu X, Gajewiak J, Tsukahara R, Fujiwara Y, Liu J, Fells JI, Perygin D, Parrill AL, Tigyi G, Prestwich GD. Dual activity lysophosphatidic acid receptor pan-antagonist/autotaxin inhibitor reduces breast cancer cell migration in vitro and causes tumor regression in vivo. Can Res. 2009; 69:5441–5449.
41. Tybulewicz VL, Henderson RB. Rho family GTPases and their regulators in lymphocytes. Nat Rev Immunol. 2009; 9:630–644. [PubMed: 19696767]
42. Chettibi S, Lawrence AJ, Stevenson RD, Young JD. Effect of lysophosphatidic acid on motility, polarisation and metabolic burst of human neutrophils. FEMS Immunol Med Microbiol. 1994; 8:271–281. [PubMed: 8004064]
43. Fulkerson Z, Wu T, Sunakura M, Vander Kooi C, Morris AJ, Smyth SS. Binding of autotaxin to integrins localizes lysophosphatidic acid production to platelets and mammalian cells. J Biol Chem. 2011; 286:34654–34663. [PubMed: 21832043]
44. Huang JH, Cardenas-Navia LI, Caldwell CC, Plumb TJ, Radu CG, Rocha PN, Wilder T, Bromberg JS, Cronstein BN, Sitkovsky M, Dewhirst MW, Dustin ML. Requirements for T lymphocyte migration in explanted lymph nodes. J Immunol. 2007; 178:7747–7755. [PubMed: 17548612]
45. Okada T, Cyster JG. CC chemokine receptor 7 contributes to Gi-dependent T cell motility in the lymph node. J Immunol. 2007; 178:2973–2978. [PubMed: 17312142]
46. Worbs T, Mempel TR, Bolter J, von Andrian UH, Forster R. CCR7 ligands stimulate the intranodal motility of T lymphocytes in vivo. J Exp Med. 2007; 204:489–495. [PubMed: 17325198]
47. Gerard A, van der Kammen RA, Janssen H, Ellenbroek SI, Collard JG. The Rac activator Tiam1 controls efficient T-cell trafficking and route of transendothelial migration. Blood. 2009; 113:6138–6147. [PubMed: 19139083]
48. Boscacci RT, Pfeiffer F, Gollmer K, Sevilla AI, Martin AM, Soriano SF, Natale D, Henrickson S, von Andrian UH, Fukui Y, Mellado M, Deutsch U, Engelhardt B, Stein JV. Comprehensive analysis of lymph node stroma-expressed Ig superfamily members reveals redundant and nonredundant roles for ICAM-1, ICAM-2, and VCAM-1 in lymphocyte homing. Blood. 2010; 116:915–925. [PubMed: 20395417]
49. Park EJ, Peixoto A, Imai Y, Goodarzi A, Cheng G, Carman CV, von Andrian UH, Shimaoka M. Distinct roles for LFA-1 affinity regulation during T-cell adhesion, diapedesis, and interstitial migration in lymph nodes. Blood. 2010; 115:1572–1581. [PubMed: 20023213]
50. Heasman SJ, Carlin LM, Cox S, Ng T, Ridley AJ. Coordinated RhoA signaling at the leading edge and uropod is required for T cell transendothelial migration. J Cell Biol. 2010; 190:553–563. [PubMed: 20733052]
51. Zhao J, He D, Berdyshev E, Zhong M, Salgia R, Morris AJ, Smyth SS, Natarajan V, Zhao Y. Autotaxin induces lung epithelial cell migration through lysoPLD activity-dependent and -independent pathways. Biochem J. 2011; 439:45–55. [PubMed: 21696367]
52. Hausmann J, Kamtekar S, Christodoulou E, Day JE, Wu T, Fulkerson Z, Albers HM, van Meeteren LA, Houben AJ, van Zeijl L, Jansen S, Andries M, Hall T, Pegg LE, Benson TE, Kasiem M, Harlos K, Kooi CW, Smyth SS, Ovaa H, Bollen M, Morris AJ, Moolenaar WH, Perrakis A. Structural basis of substrate discrimination and integrin binding by autotaxin. Nat Struct Mol Biol. 2011; 18:198–204. [PubMed: 21240271]
53. Nishimasu H, Okudaira S, Hama K, Mihara E, Dohmae N, Inoue A, Ishitani R, Takagi J, Aoki J, Nureki O. Crystal structure of autotaxin and insight into GPCR activation by lipid mediators. Nat Struct Mol Biol. 2011; 18:205–212. [PubMed: 21240269]
54. Goetzl EJ, Rosen H. Regulation of immunity by lysosphingolipids and their G protein-coupled receptors. J Clin Invest. 2004; 114:1531–1537. [PubMed: 15578083]

55. Yanagida K, Masago K, Nakanishi H, Kihara Y, Hamano F, Tajima Y, Taguchi R, Shimizu T, Ishii S. Identification and characterization of a novel lysophosphatidic acid receptor, p2y5/LPA6. J Biol Chem. 2009; 284:17731–17741. [PubMed: 19386608]

56. Jiang G, Xu Y, Fujiwara Y, Tsukahara T, Tsukahara R, Gajewiak J, Tigyi G, Prestwich GD. Alpha-substituted phosphonate analogues of lysophosphatidic acid (LPA) selectively inhibit production and action of LPA. Chem Med Chem. 2007; 2:679–690. [PubMed: 17443831]

57. Rosen H, Sanna MG, Cahalan SM, Gonzalez-Cabrera PJ. Tipping the gatekeeper: S1P regulation of endothelial barrier function. Trends Immunol. 2007; 28:102–107. [PubMed: 17276731]

58. Schwab SR, Cyster JG. Finding a way out: lymphocyte egress from lymphoid organs. Nat Immunol. 2007; 8:1295–1301. [PubMed: 18026082]

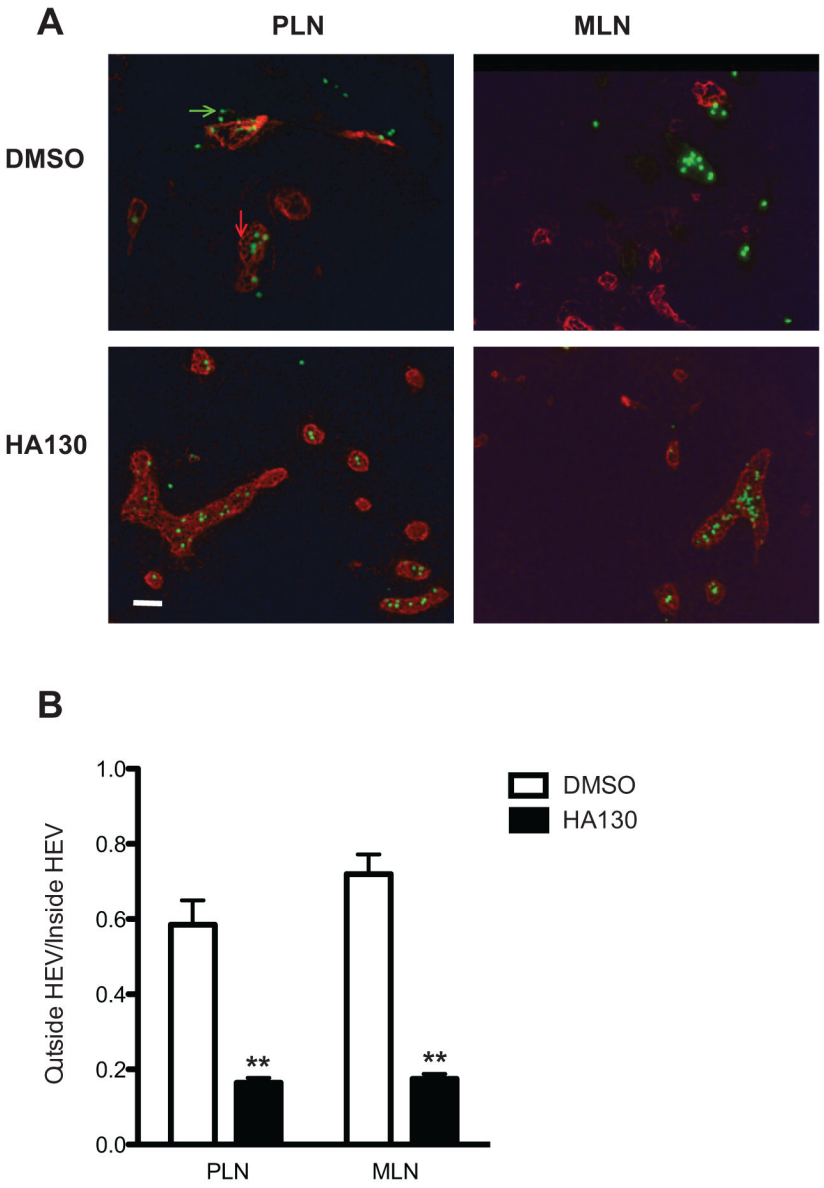

Figure 1. HA130 impedes T cell entry into lymph nodes

(A) HEVs in PLN and MLN sections were stained with MECA 79. Representative images of CFSE-labeled T cells in control and HA130-treated mice are shown after intravenously injection of CFSE-labeled T cells. Scale bar = 50 μM. (B) Bar graphs for PLN and MLN showing mean ratios ± SDs of CFSE-labeled cells "outside HEVs" to those "inside HEVs". 2 mice were processed per experiment with 6 non-consecutive sections of 2 MLNs and 3 PLNs evaluated for each mouse. Green arrow indicates CFSE-labeled T cell, and red arrow indicates MECA-79 stained HEV. The data shown represent the pooled results from 3 experiments (3 mice of each group). * *denotes $p < 0.01$ versus DMSO control.

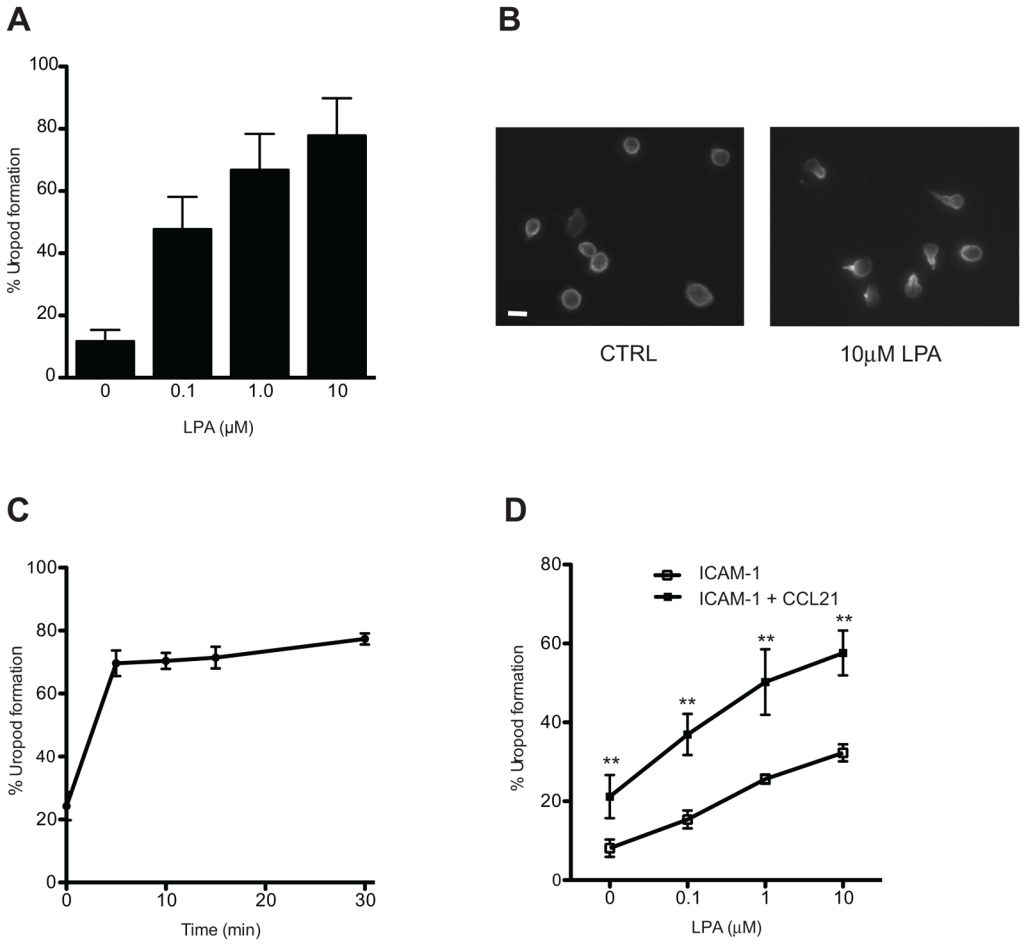

Figure 2. LPA induces the rapid polarization of T cells

(A) TK1 lymphoma cells were allowed to settle on ICAM-1 substratum in the presence of the indicated concentration of LPA. After 7 min, percent of cells that became polarized was determined as defined by CD44 accumulation in uropods. (B) CD44 staining of TK1 cells after 7 min exposure to 10 μM LPA (right panel) or buffer alone (left panel). Scale bar = 10 μM. (C) Time course of TK1 polarization response to 0.1 μM LPA. (D) Naïve mouse T cells were allowed to settle on substratum of ICAM-1 or ICAM-1 with co-immobilized CCL21 (200 ng/ml input). After 7 min, polarization was determined based on accumulation of CD43 into uropods. CD43 was used instead of CD44 because of the low expression of the latter on naïve T cells. In A, C, and D, means and SDs are shown and are based on 3 replicate wells. ** denotes $p < 0.01$ for comparison of uropod formation with CCL21 vs. without CCL21. Data are representative of 3 independent experiments.

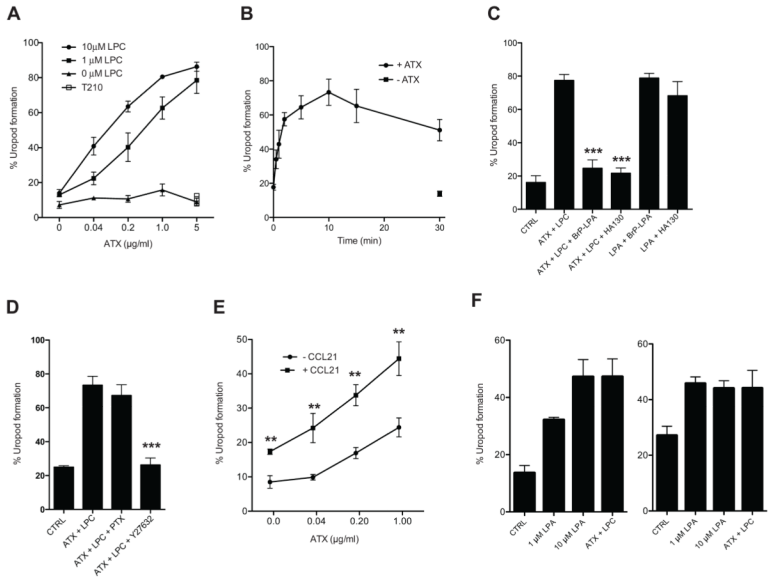

Figure 3. ATX in the presence of LPC induces polarization of T cells

(A) TK1 cells were allowed to settle on ICAM-1 substratum in the presence of the indicated concentration of ATX with (1 μM, 10 μM) or without LPC in solution. □denotes response to 5 μg/ml of T210A with 10 μM LPC. After 7 min, percent of cells that became polarized was determined by CD44 accumulation in uropods. For all ATX concentrations except 5 μg/ml: 10 μM LPC > 1 μM > 0 LPC with $p < 0.01$ by ANOVA. For 5 μg/ml ATX: 1 and 10 μM LPC > 0 LPC with $p < 0.001$ by ANOVA. (B) Time course of TK1 polarization response to 1 μg/ml ATX and 1 μM LPC in solution. ■indicates response to 1 μM LPC alone. (C) TK1 polarization response to ATX (5 μg/ml) plus LPC (1 μM) or to LPA (1 μM) in the presence of either BrP-LPA (10 μM) or HA130 (0.3 μM). Uropod response was measured after 7 min. CRTL, no additions. *** denotes $p < 0.001$ for comparisons of ATX/LPC vs. ATX/LPC + HA130 and ATX/LPC + BrP-LPA. (D) TK1 polarization response to ATX (5 μg/ml) plus LPC (1 μM) when cells were treated with pertussis toxin (200 ng/ml) or Y27632 (10 μM). *** denotes $p < 0.001$ for comparison of ATX/LPC vs. ATX/LPC + Y27632. (E) Naïve T cell polarization response (CD43 uropod assay) to the indicated concentration of ATX in solution with 1 μM LPC present. The substratum consisted of ICAM-1 with or without co-immobilized CCL21 (200 ng/ml). ** denotes $p < 0.01$ for comparison of uropod formation with CCL21 vs. without CCL21. (F) Human blood T cells (left) and neutrophils (right) were allowed to settle on ICAM-1 coated wells in the presence of LPA or ATX (1 μg/ml) with 1 μM LPC. Uropod formation was determined by staining for the accumulation of CD44. In all panels, means and SDs are shown and are based on 3 replicate wells. Data are representative of 3 independent experiments with the exception of panel F which was performed twice.

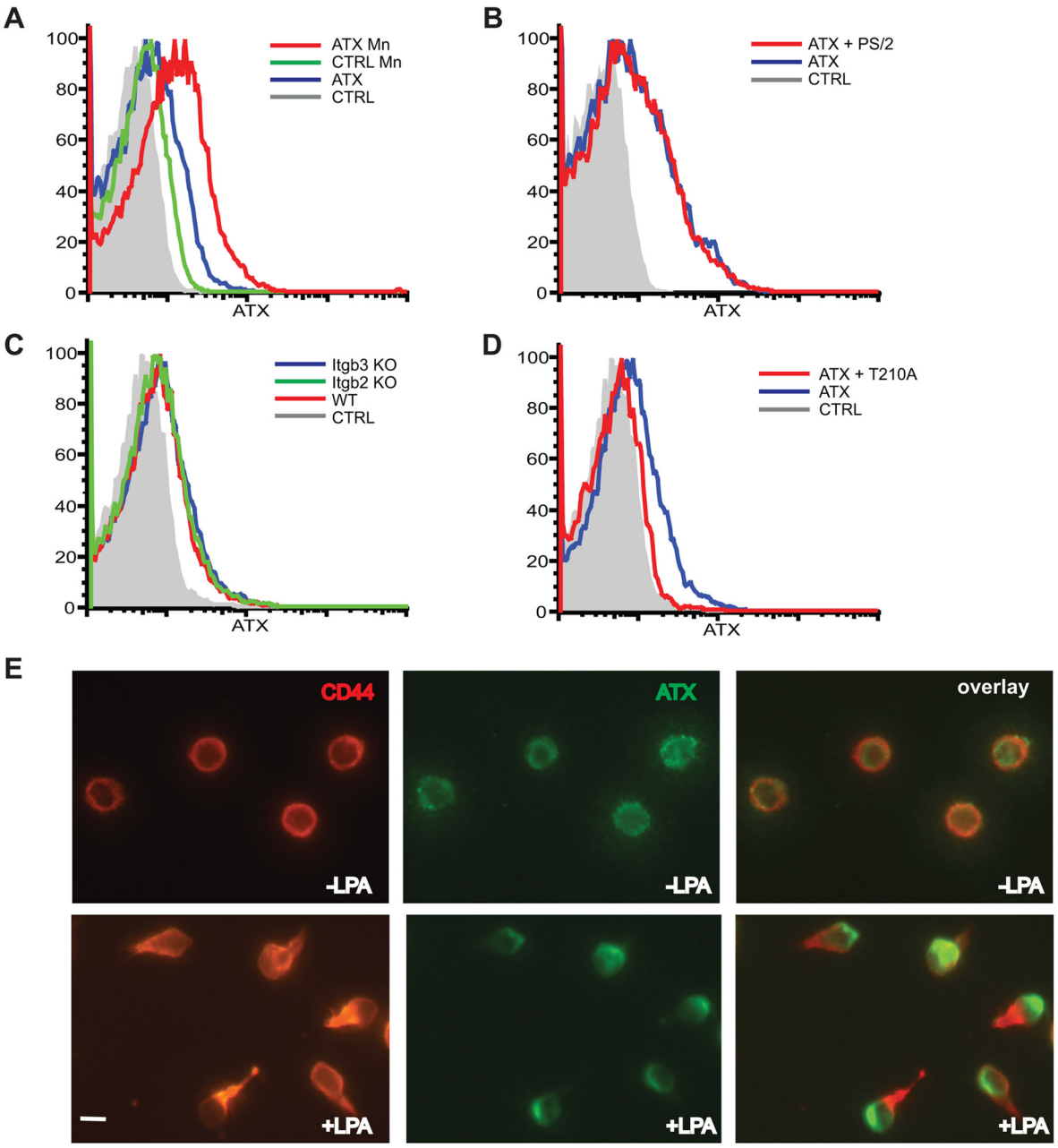

Figure 4. Binding of ATX to T cells

(A) Flow cytometry analysis of b-ATX staining of mouse T cells in the presence (red) or absence of Mn^{+2} (blue trace). CTRL here and in panels **B–D** denotes staining with b-ATX omitted. (B) b-ATX staining (with Mn^{+2} present) of T cells in the presence or absence of PS/2, an anti α4 integrin antibody. (C) b-ATX staining (with Mn^{+2} present) of T cells from wild-type mice, β2-deficient T cells (*Itgβ2* null mice), and β3-deficient T cells (*Itgβ3* null mice) (D) b-ATX staining (with Mn^{+2} present) of T cells in the presence or absence of a 10-fold excess of T210A. (E) Fluorescent imaging of TK1 cells stained with b-ATX (green) and CD44 (red). Top row shows rounded cells bound to substratum and bottom row shows polarized cells (induced with 1 μM LPA). Scale bar denotes 10 μM. Data are representative of at least 4 independent experiments

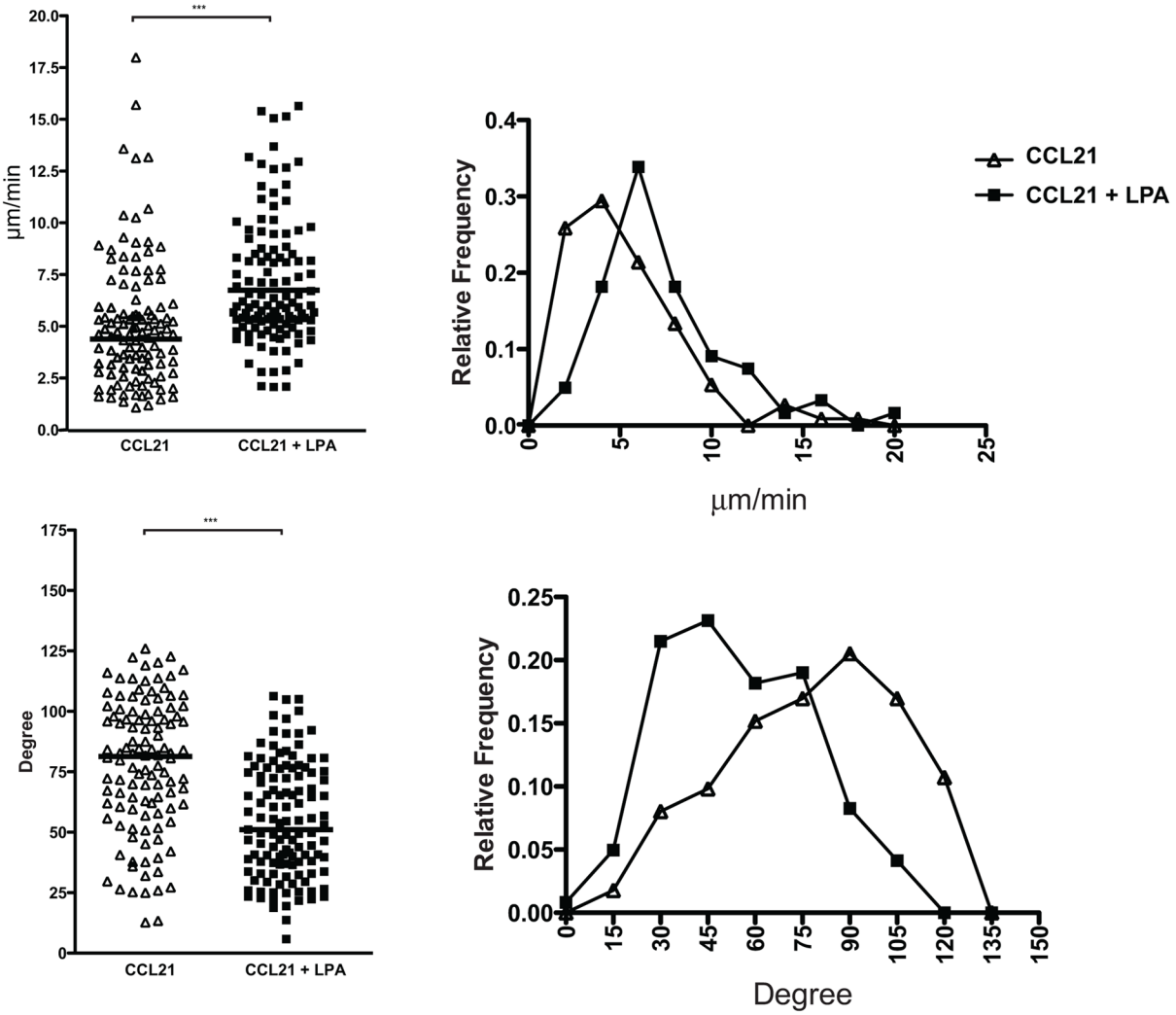

Figure 5. LPA induces motility of naïve T cells.

Naïve GFP+ CD4+ OTII T cells were seeded with or without 1 μM LPA onto a chamber coated with ICAM and CCL21. Median velocity (top) and turning angle (bottom) of each cell were measured and are shown in dot and relatively frequency plots. Data are representative of 3 independent experiments. *** denotes $p < 0.001$.

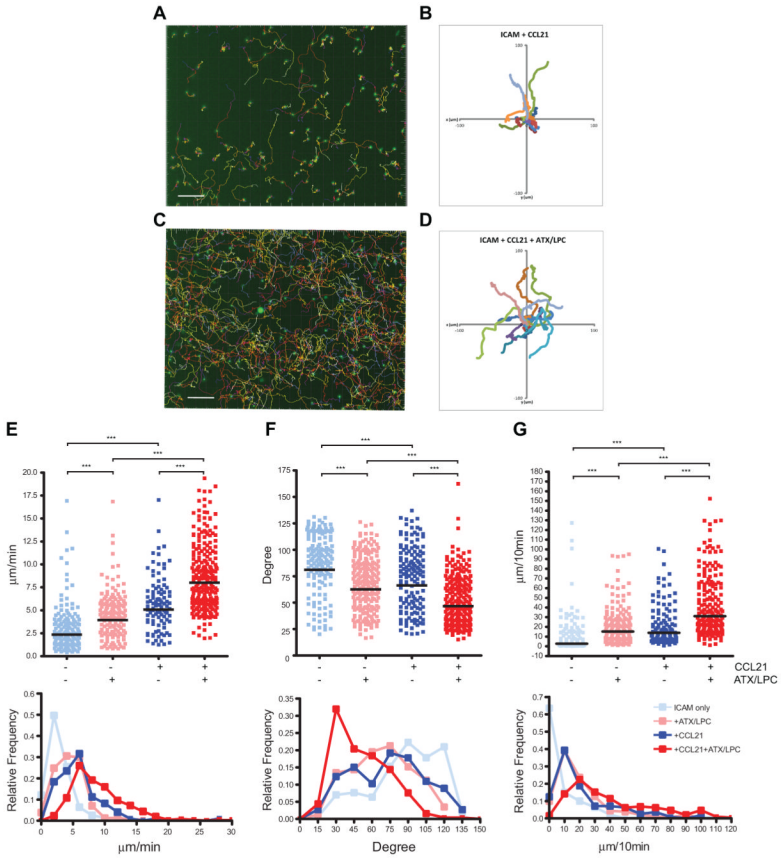

Figure 6. ATX induces motility of naïve T cells.

Naïve GFP+ CD4+ OTII T cells were seeded onto a crawling chamber coated with 3 μg/ml ICAM-1 + 400 ng/ml CCL21 with or without 1 μg/ml ATX plus 10 μM LPC in solution. T cells were imaged every 15 sec for 15 min and tracked by Imaris software. Cell tracks are shown for a 10 min period on (A, B) an ICAM-1 plus CCL21 substratum and on (C, D) an ICAM-1 plus CCL21 substratum in the presence of 1 μg/ml ATX and 10 μM LPC in solution. A and C show all of the tracks (> 100 cells per experimental set); B and D show 10 randomly chosen sample tracks for a 10 min period of migration referenced to the origin of each cell. Median velocity (E), turning angle (F), and average total displacement (G) of each cell were measured over 10 min and are shown in dot (top) and relative frequency plots (bottom). *** denotes $p < 0.001$ for the indicated comparison as determined by ANOVA. Data are representative of 3 independent experiments.

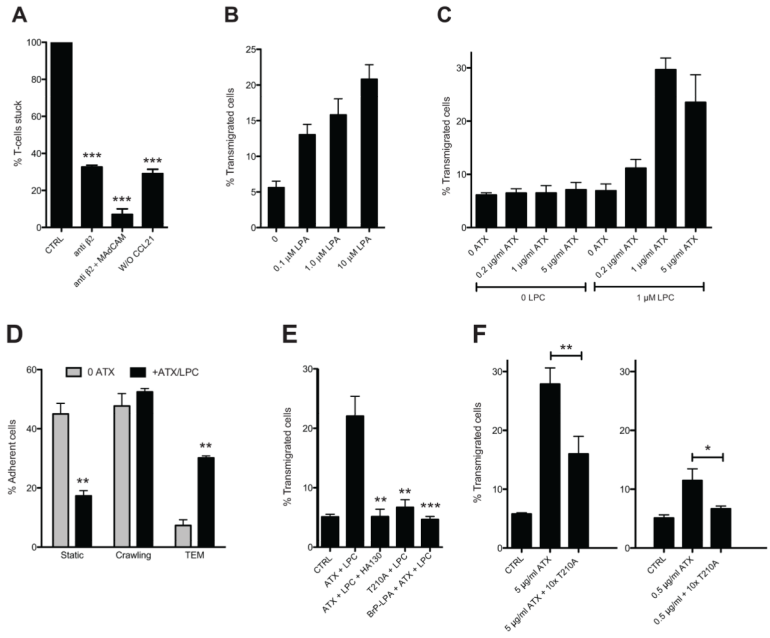

Figure 7. LPA and ATX promote TEM of T cells in a flow chamber

(A) Mouse T cells were allowed to adhere to TNF-α stimulated and CCL21-coated bEnd.3 cells under shear stress in the presence of buffer alone (CTRL), anti-β2 integrin and anti-MAdCAM-1 antibodies, or without CCL21 pre-treatment of the EC monolayer. After a 10 min period of flow, the number of adherent T cells was normalized to the number of adherent cells with buffer alone. *** denotes $p < 0.001$ for treatment compared to CTRL. (B) LPA was added to the flow chamber and the number of T cells undergoing TEM across the bEnd.3 monolayer was determined over the 30 min period of flow and computed as a percentage of the number of adherent cells at 10 min ("percent TEM"). (C) ATX was added to the chamber with or without LPC and the number of T cells undergoing TEM was determined as above. (D) The flow chamber contained either buffer or ATX (5 μg/ml) plus LPC (1 μM). The behavior of adherent T cells was categorized as either "static", "crawling" or "undergoing TEM". The percent of cells in each category was compared with or without ATX/LPC. ** denotes $p < 0.01$ for ATX/PLC vs. no treatment. (E) TEM of T cells across the bEnd.3 monolayer was measured in the presence of buffer alone (CTRL), ATX/LPC (5 μg/ml/1 μM), ATX/LPC plus HA130 (0.3 μM), ATX/LPC plus BrP-LPA (10 μM) or T210A/LPC (5 μg/ml/1 μM). *** denotes $p < 0.001$ and ** $p < 0.01$ for comparison of the indicated treatment with ATX/LPC. (F) TEM of T cells across the bEnd.3 monolayer was measured as above in the presence of buffer alone (CTRL), ATX at 5 μg/ml, ATX at 5 μg/ml plus 10-fold T210A, 0.5 μg/ml ATX, or 0.5 μg/ml ATX plus 10-fold excess of T210A. The left and right panels were separate experiments. All ATX conditions also included 1 μM LPC. ** denotes $p < 0.01$, * $p < 0.05$ for the indicated comparison. Means and SDs are shown and are based on 3 replicate determinations. Data are representative of 3 independent experiments.